2005

The Role of Feeding Behavior in Sustaining Copepod Populations in the Tropical Ocean

J. D. Wiggert
Old Dominion University

A. G. E. Haskell

G.-A. Paffenhofer

E. E. Hofmann
Old Dominion University, ehofmann@odu.edu

J. M. Klinck
Old Dominion University, jklinck@odu.edu

Original Publication Citation

Wiggert, J. D., Haskell, A. G. E., Paffenhofer, G. A., Hofmann, E. E., & Klinck, J. M. (2005). The role of feeding behavior in sustaining copepod populations in the tropical ocean. *Journal of Plankton Research, 27*(10), 1013-1031. doi:10.1093/plankt/fbi090

JOURNAL OF PLANKTON RESEARCH | VOLUME 27 | NUMBER 10 | PAGES 1013–1031 | 2005

The role of feeding behavior in sustaining copepod populations in the tropical ocean

J. D. WIGGERT[1]*, A. G. E. HASKELL[2], G.-A. PAFFENHÖFER[3], E. E. HOFMANN[1] AND J. M. KLINCK[1]

[1]CENTER FOR COASTAL PHYSICAL OCEANOGRAPHY, OLD DOMINION UNIVERSITY, NORFOLK, VA 23508-2026, USA, [2]RESEARCH SYSTEMS, INC., 4990 PEARL EAST CIRCLE, BOULDER, CO 80301, USA AND [3]SKIDAWAY INSTITUTE OF OCEANOGRAPHY, 10 OCEAN SCIENCE CIRCLE, SAVANNAH, GA 31411, USA

*CORRESPONDING AUTHOR: jwiggert@ccpo.odu.edu

Received May 12, 2005; accepted in principle July 26, 2005; accepted for publication October 20, 2005; published online November 22, 2005

Communicating editor: R.P. Harris

A fundamental question regarding marine copepods is how the many species coexist and persist in the oligotrophic environment (i.e. Hutchinson's paradox). This question is addressed with a stochastic, object-oriented Lagrangian model that explicitly simulates the distinct foraging behaviors of three prominent tropical species: Clausocalanus furcatus, Paracalanus aculeatus *and* Oithona plumifera. *The model also individually tracks all prey cells. Each particle's motion combines sinking, turbulent diffusion and active swimming when applicable. The model successfully simulates observed size-partitioned carbon uptake rates. Based on the model results, the wide-ranging translational ambit employed by* C. furcatus *is best suited for the acquisition of passive prey while the relatively stationary behavior of* O. plumifera *promotes the capture of larger, quickly sinking cells. The model results further suggest that the slow velocities and feeding current employed by* P. aculeatus *are best suited for acquiring the smallest cells though it also has a slight advantage over* C. furcatus *in acquiring the largest prey. A resource threshold, at a prey concentration of 530 cells* mL^{-1}*, is consistently exhibited by all three modeled species. Overall, these results imply that the size-partition preferences due to their different foraging behavior contribute to the coexistence of these three species.*

INTRODUCTION

Numerous species of plankton populate the world's oceans. However, in the tropical open ocean there is a limited number of ecological niches. Even so, a diverse array of planktonic organisms is observed to flourish. Since it challenges a fundamental ecological tenant that dates back to Darwin (i.e. competitive exclusion), this characteristic of the oceanic ecosystem has intrigued oceanographers for decades and has been termed the paradox of the plankton. Hutchinson (Hutchinson, 1961) phrased this paradox as: 'How is it possible for a number of species to coexist in a relatively isotropic or unstructured environment all competing for the same sorts of materials?'. While he was specifically referring to the pelagic environment's autotrophic population, such a question could also be applied to heterotrophic organisms. Assessing Hutchinson's paradox has remained a topical issue over the years. One theory, termed contemporaneous disequilibrium, postulates that the actions of fluid turbulence result in sufficient environmental variability as to prevent the formation of stable niches that could become dominated by a single species (Richerson *et al.*, 1970).

In his re-visitation of the paradox, Ghilarov (Ghilarov, 1984) suggests that an alternative explanation, termed the 'coexistence principle', may be more appropriate. This principle is based on the general ecological observation that taxonomically similar species often demonstrate similar distribution patterns. For example, an analysis of copepod species in the central gyre of the North Pacific suggests that they are typically generalists (Hayward and McGowan, 1979). Moreover, tight predator–prey couplings were uncommon, and species-specific niches with minimal overlap were not observed. The species assemblage in this region remained unaffected by a transitory climatic event that significantly perturbed environmental conditions, which led to the conclusion that disturbance–perturbation theory was

This paper is one of six on the subject of the role of zooplankton predator–prey interactions in structuring plankton communities.

doi:10.1093/plankt/fbi090, available online at www.plankt.oxfordjournals.org

not applicable as a means of producing species diversity (McGowan and Walker, 1985). In regions exhibiting more pronounced vertical environmental gradients, layering of species assemblages has been documented, which has led to the suggestion that the range of conditions results in a multitude of niches capable of supporting numerous species and that contemporaneous disequilibrium may further promote diversity by operating within localized depth zones (Longhurst, 1985). Ongoing advances in optical and acoustical sampling capabilities have demonstrated that such vertical layering of community structure associated with density discontinuities can occur on the scale of O (10^{-1} to 1) meters while extending several kilometers horizontally and persisting for several days. It has been suggested that this partitioning into microenvironments may contribute to the maintenance of species diversity (McManus *et al.*, 2003).

Zooplankton play a crucial and multifaceted role in the processing of biogenic material in the pelagic environment, yet our present understanding of their specific ecological function remains relatively rudimentary. Recently, the Second Marine Zooplankton Colloquium (MZC2) identified three basic research foci, one of which consisted of developing a better characterization of the role of zooplankton in oceanic biogeochemical cycling (MZC2, 2001). Budgets of daily nutrient rations indicate that copepods must practice omnivory to meet their metabolic and dietary requirements (Cowles and Fessenden, 1995; Roman and Gauzens, 1997). The most prominent copepod food source may be protozoa (i.e. microzooplankton), and copepod grazing pressure can propagate as a trophic cascade that influences the abundance of other ecosystem constituents (Calbet and Landry, 1999). This represents top–down control of the lower trophic levels, whereas zooplankton excretion acts as a bottom-up stimulation of the food web. Thus copepods have varied impact on constituent concentrations. In addition, copepods are commonly identified as prominent contributors to the export of biogenic carbon to the deep ocean because of the elevated sinking rates of their fecal pellets (Banse, 1994; Roman *et al.*, 1995; Al-Mutairi and Landry, 2001). However, it has also been observed that cyclopoid coprophagy can mitigate detrital fluxes to the deep ocean (Svensen and Nejstgaard, 2003; Huskin *et al.*, 2004), and coprophagy in general may result in a more nutritionally complete ration for copepod species (Roman, 1984; Kleppel, 1993).

Within the context of copepod diversity in the tropical oceans, Hutchinson's paradox could be recast as: 'How do the many copepod species exist, co-exist, and persist within an environment characterized by dilute plankton concentrations?'. This is a primary motivation of the work reported here, which entails developing a detailed behavioral model that is used to investigate how a diverse copepod assemblage is maintained under typical oligotrophic conditions. This modeling approach consists of developing and applying a Lagrangian scheme that incorporates explicit foraging behavior for three separate copepod species. These species are typically abundant in the tropical/subtropical oligotrophic ocean and employ distinct methods of prey acquisition (Paffenhöfer, 1993; Gallienne and Robins, 2001). The three species and the associated foraging methods that have been emulated in the model are as follows. *Clausocalanus furcatus* is a fast continuous swimmer that loops repetitively then displaces vertically before reestablishing its characteristic looping motion (Mazzocchi and Paffenhöfer, 1999). *Paracalanus aculeatus* is a slow continuous swimmer that generates a feeding current to entrain potential food particles and perceives food at a distance by cehmoreception (Paffenhöfer, 1984, 1998). *Oithona plumifera* is an ambush predator that uses its long-feathered setae to sense the hydrodynamical signals of motile particles at a distance (Svensen and Kiørboe, 2000). After shifting every few seconds by moving obliquely upward, potential food particles are perceived as these copepods slowly sink, remaining motionless with their bodies typically oriented horizontally (Paffenhöfer and Mazzocchi, 2002).

Here, the first results from this stochastic Lagrangian model are presented. The model's specific details and the numerical experiments performed for this 'proof-of-concept' study are described. This is followed by a comparison of the simulated foraging behavior and uptake rates with observations and rate measurements from several recent studies. Results from the model are then used to assess how well the three species are able to survive over a range of prey concentrations and to investigate how their distinct foraging behaviors affect their grazing success.

METHOD

Particle motion and copepod ambits

The stochastic, object-oriented Lagrangian model is used to individually track particles that represent the members of a realistic plankton population and the attendant group of foraging copepods. The latter employ species-specific motions and sampling strategies. Equation (1) describes the trajectory of a given particle at location $\vec{X}_i$.

$$\frac{\mathrm{d}\vec{X}_i}{\mathrm{d}t} = \vec{U}_i \tag{1}$$

The subscript denotes an individual particle (either prey or copepod) while the associated velocity ($\vec{U}_i$) entails the superposition of a passive sinking speed, a random component meant to emulate isotropic turbulence and an active swimming speed where applicable. In the equations that follow, the subscript is dropped, and it is assumed that each particle has distinct motion components. The model is currently used to simulate copepod ambits for 1 h, so physiological processes of growth and reproduction are not included, and diel, large-scale vertical migrations have not been incorporated. Advection is assumed to affect all particles similarly and is therefore not explicitly included.

Particle sinking (w_s) is estimated for individual phytoplankton using a modified form of the Stokes equation for particles sinking within a fluid medium [equation (2)], where g is gravitational acceleration, $\Delta\rho$ is the typical difference in density between phytoplankton cells and seawater, μ is the viscosity of seawater and Φ is a form resistance factor. Cell diameter (d_C) is considered an equivalent cell diameter (*ESD*), and the distribution of d_C for the prey field (i.e. its size spectrum) is uniquely determined when each numerical experiment is initiated (see *Initialization of the modeled potential prey-size spectrum*).

$$w_S = \frac{g d_C^2 B^R \Delta\rho}{18\mu\Phi}, \quad \text{where } 0.9 \le B^R \le 1.1 \tag{2}$$

The resistance factor accounts for deviations from Stokes Law that manifest between velocities realized by an essentially spherical plankter and that obtained by an idealized sphere of similar volume and density (Padisák *et al.*, 2003). The modification to the density difference (B^R) represents natural cell density variability within the plankton population, where the superscript here (and below) denotes that this is a randomized component within the indicated bounds. The maximum sinking velocity for a 50-μm cell has been set to 2.1 m day^{-1}, based on published observations (Mann and Lazier, 1996). Cell-buoyancy adaptations in response to environmental conditions (e.g. irradiance levels or nutrient concentrations) are not explicitly accounted for, and it is assumed that no cells are senescent. Since *C. furcatus* and *P. aculeatus* are continuous swimmers, a sinking rate is not applied to these two species. During its foraging periods *O. plumifera* sinks with a velocity of 24.1 m day^{-1}, a value that is based on observational studies (Paffenhöfer and Mazzocchi, 2002).

Diffusion ($\vec{u}_D$), or drifting, of individual copepods and plankton due to turbulence is presently represented as an additional random component to the velocity vector. This turbulent velocity component is applied as a maximum diffusion speed (D), the magnitude of which is modified for each direction by a set of random amplitudinal coefficients ($\vec{\beta}^R$) that are uniformly distributed between –1 and 1. A new set of $\vec{\beta}^R$ is determined for each individual at every time step.

$$\vec{u}_D = \vec{\beta}^R D \tag{3}$$

Directed motion is only applied to the zooplankton and is prescribed for individual species as swimming with or without pauses. A copepod's ambit can be set to simulate various characteristic behaviors that range from large jumps separated by periods of sinking to swimming continuously in tight spirals. If a copepod does not move continuously, equation (4) contributes to its ambit. The duration of each motion episode (τ_S) is calculated from a base time duration (τ_B) modified by a uniformly distributed perturbation (ε_S^R), the magnitude of which is bounded ($\varepsilon_S^{\max}$). This bound's value depends on species and the emulated motion but represents at most a modification to τ_B of ±20%.

$$\tau_S = \tau_B\left(1 \pm \varepsilon_S^R\right), \quad \text{where } 0 \le \varepsilon_S^R \le \varepsilon_S^{\max} \text{ and } 0.1 \le \varepsilon_S^{\max} \le 0.2 \tag{4}$$

For copepods that move intermittently, they are assumed to be either at rest or their maximum speed (C_S) for the duration of each motion event, where C_S is based on observations (Table I). These motion events include either jumping, which entails a translational shift and possibly a heading modification, or somersaulting, which involves remaining in place and acquiring a new directional heading.

Each copepod's heading is specified by a zenith angle (θ) and an azimuth angle (ϕ). Equations (5) and (6) prescribe these angles through modification of a maximum deviation (θ_M,ϕ_M) by a uniformly distributed random value ($\varepsilon_{\theta,\phi}^R$). Both the values of the maximum angular deviations and the range of the perturbations vary depending on species and whether a given copepod is currently swimming or undergoing a somersaulting episode.

$$\frac{\mathrm{d}\theta}{\mathrm{d}t} = \theta_M\left(2\varepsilon_\theta^R - 1\right), \quad \text{where } 0 < \varepsilon_\theta^R < 1 \tag{5}$$

$$\frac{\mathrm{d}\phi}{\mathrm{d}t} = \phi_M\left(2\varepsilon_\phi^R - 1\right), \quad \text{where } 0.5 < \varepsilon_\phi^R < 1 \tag{6}$$

Table I: Observed species characteristics

Species	Copepod weight (μg C)	Copepod speed (C_S) (mm s^{-1})	Feeding current (mm s^{-1})	Planview area (mm^2)	Volume perceived (stationary) (mm^3)	Volume sampling rate (mm^3 s^{-1})
Clausocalanus furcatus	3.6	10.00	0.00	0.09	–	0.86
Paracalanus aculeatus	4.2	0.70	0.80	2.30	–	2.89
Oithona plumifera	2.6	0.28[a]	0.00	1.48/0.78[b]	0.67/0.52[c]	0.64

The weight given for *C. furcatus* is from Mazzocchi and Paffenhöfer (Mazzocchi and Paffenhöfer, 1998), for *P. aculeatus* is from Paffenhöfer *et al.* (Paffenhöfer *et al.*, 2003) and for *O. plumifera* is from Klekowski *et al.* (Klekowski *et al.*, 1977).
[a]Represents a sinking velocity.
[b]Represents ventral sensory regions.
[c]Represents abdomen sensory regions.

The new heading values thus prescribe the updated velocity vector for the copepod's ambit [equation (7)].

$$\vec{u}_A = \begin{pmatrix} C_S \cos\phi \sin\theta \\ C_S \sin\phi \sin\theta \\ C_S \cos\theta \end{pmatrix} \quad (7)$$

Calculation of the new position then follows by applying the new velocity components $(w_S, \vec{u}_D, \vec{u}_A)$ to $\vec{U}_i$ in equation (1).

Prey perception and particle ranking

For all three species, their velocities in the model were made equivalent to their observed velocities. In order to account for variations in perception and foraging strategies, area(s) of perception (AOP) were prescribed for each species. These are defined by a radius of influence (*ROI*) that extends away from the copepod and an angle of influence (*AOI*) that extends to either side of the copepod's direction heading (Fig. 1). Depending on the species to be emulated, either one or two AOPs have been defined. These account for perception from the group(s) of antennae/setae that in the model configuration are considered to extend from the front, and possibly also the rear, of a given copepod. Of the three modeled species, only *O. plumifera* was provided with the additional rear AOP since it has extensive multiple sensory apparatus.

The prescribed AOP in the model are not necessarily identical to those determined in laboratory studies. This was necessary in order to account for the differences between nature and a model that is necessarily discretized. For example, the observed foraging behavior of *C. furcatus* is to move constantly at high velocity and to identify potential prey through nearly direct contact. To emulate this behavior without the need for an infinitesimally small model time step, a long, narrow AOP was defined so that cells within a cone that extends forward along a given individual's heading would be considered. Thus for each time step, an entirely new distribution of potential food particles is acquired. In the case of *P. aculeatus*, instead of increasing its forward velocity and skewing the resulting translational ambit, its *ROI* was extended to account for the additional volume perceived as a result of the feeding current generated by this species. Finally, the complex sensory apparatus conguration of *O. plumifera* is not reproduced due to the need to simply define AOP within a modeling context. The observed sensing characteristics of each copepod species are listed in Table I. The applied values of *ROI* and *AOI* are provided in Table II. While it is apparent that the planview area may differ, the combination of velocity and modeled sensing region(s) results in modeled volume sampling rates that are essentially identical to those observed in the laboratory experiments (Table I).

All particles encompassed by the modeled AOP were considered as potential prey. For each particle type, an initial rank was defined that reflects observed preferences for each type of prey by each copepod species. Each particle's rank was reduced by two non-dimensional perception factors ($\pi_{1,2}$) that accounted for a given cell's size and distance from the copepod. The size-based factor (π_1) is defined as follows.

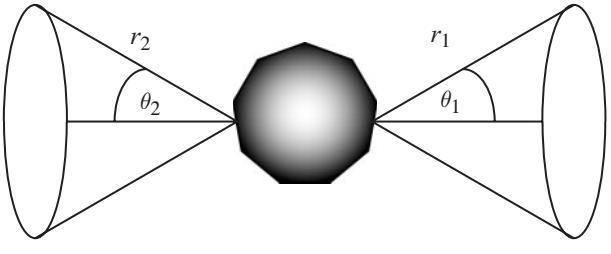

Fig. 1. Modeled copepod sensory regions. The values for the radius of influence (*ROI*) (r_1 and r_2) and angle of influence (*AOI*) (θ_1 and θ_2) for each copepod species are provided in Table II.

Table II: Modeled sensing region(s)

Species	*ROI* (r) (mm)	*AOI* (θ) (degrees)	Planview area (mm^2)	Volume perceived (stationary) (mm^3)	Volume sampling rate ($mm^3\ s^{-1}$)
Clausocalanus furcatus	4.00	4.58	0.32	0.43	0.86
Paracalanus aculeatus	1.15	90.00	4.13	3.16	2.89
Oithona plumifera	3.50/1.22	7.0/30.0	1.50/0.78[a]	0.66/0.55[b]	0.64

The radius of influence (*ROI*) and angle of influence (*AOI*) listed here, respectively, correspond to the model copepod characteristics $r_{1,2}$ and $\theta_{1,2}$ shown in Fig. 1.
[a]Represents ventral sensory regions.
[b]Represents abdomen sensory regions.

$$\pi_1 = \frac{\{1+\tanh[(d_C - a_1 d_P)/b_1]\}\{1-\tanh[(d_C - a_2 d_P)/b_2]\}}{\{1+\tanh[d_P(1-a_1)/b_1]\}\{1-\tanh[d_P(1-a_2)/b_2]\}} \quad (8)$$

Here, $a_1 = 0.175$, $b_1 = 5.0$, while $a_2 = 2.0$, $b_2 = 4.0$ and $d_P = 40$ μm. Thus, the size of each particle (d_C) helps define how readily it is perceived. The form of π_1 at small particle sizes is illustrated in Fig. 2, and it can be seen that this is analogous to the observation-based cell capture efficiency developed by Bartram (Bartram, 1980). The break in the curve at 6.4 μm in Fig. 2 is introduced to illustrate the minimum cell size threshold when no other perception modifiers contribute. The 6.4-μm threshold applied here is somewhat lower than the 8-μm sampling cutoff reported for somewhat larger copepod species (Gaudy *et al.*, 2003). While there is evidence that capture efficiency is linked to feeding appendage morphology (Nival and Nival, 1976), d_P was held constant since appropriate quantification of how this efficiency varies among the three species is lacking. As d_P is lowered, the smaller plankton become more accessible while the larger cells become less accessible. The need to employ a smoothly varying switch led to the choice of the functional form used in equation (8). Its numerator is a essentially a boxcar filter for preferred cell size with limits set by d_P while the denominator ensures that π_1 is ≤ 1. Thus, through equation (8), a preferred prey partition can be prescribed for each individual grazer. In future experiments, this will be one means of incorporating distinctions between the foraging activity of growing copepodites and adult copepods.

The second perception factor (π_2) varies linearly with distance from the copepod. The lower bound for π_2 (0.8) is reached at the maximum *ROI* for a given species. These two perception factors are multiplied by the particle's initial rank and, if this remains above a prescribed minimum preference threshold, the particle is then consumed. Otherwise, the particle is returned to the pool of potential prey for the next iteration. In the perception example shown in Fig. 2, if a particle's initial rank is reduced by >55% then it has fallen below the copepod's preference threshold and is not consumed. However, it should be noted that this percent reduction is not constant as it depends on the relative values chosen for the initial rank and minimum preference threshold, both of which can depend on copepod and/or plankton species.

In the specific case of *O. plumifera*, potential prey must also exceed a minimum velocity so as to generate a hydrodynamic signal sufficient to be perceived by the setae extending from the first antennae or abdomen (Paffenhöfer and Mazzocchi, 2002). The choice of this velocity threshold made use of the only set of field

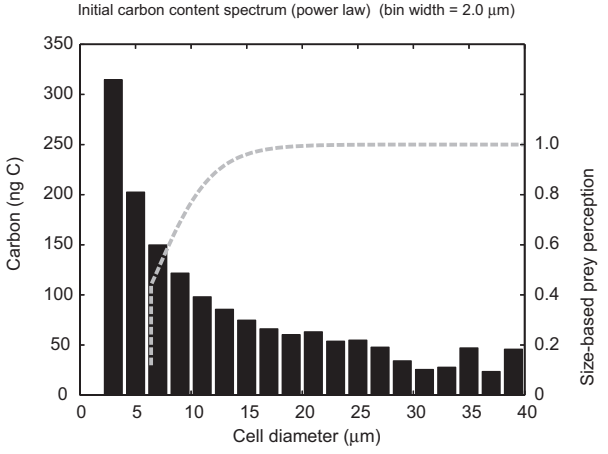

Fig. 2. A typical initial carbon content spectrum for copepod prey. The actual distribution for a given model run will differ slightly since this spectrum is randomly generated at the start of each numerical experiment. The size-partitioned distribution of prey that coincides with this example carbon content spectrum is provided in Table III. The size-based prey perception factor [π_1, equation (8)] is also shown. This function is continuous through the lowest cell equivalent cell diameter (*ESD*). The break in the curve at 6.4 μm is imposed to illustrate the lower prey size threshold that is enforced by the model's prey-ranking method.

observations of percent body weight metabolized per day that includes all three modeled copepod species (Klekowski *et al.*, 1977). The procedure used to determine this velocity threshold is detailed in *Calibration of AOP parameter settings against observed grazing rates*. The inclusion of this additional criterion for *O. plumifera* is touched on here to explain how potential prey were identified for consumption. The application of the ranking method described here provided the means by which the model emulated the different sensory methods (e.g. chemosensory or hydrosensory) employed by the copepods and the spatial degradation of the chemical and hydrodynamic signals emitted by the plankton.

Initialization of the modeled potential prey-size spectrum

The initial particle size distribution for the modeled potential prey is appropriate for the pelagic tropical/subtropical ocean as it is based on summertime plankton size spectra observed in the Sargasso Sea (Paffenhöfer *et al.*, 2003). For each experiment, the plankton-size spectrum was initialized as a transformed set of uniform deviates with sizes of 2- to 80-μm *ESD*. This transformation was derived from a power law curve fit to the mean size spectrum for cast 11a reported in Paffenhöfer *et al.* (Paffenhöfer *et al.*, 2003), for which an observed concentration of 0.4 cells mL^{-1} for the 20- to 40-μm size class has since been obtained (unpublished data). A unique particle size distribution is created when each model run is initiated, with the total number of cells corresponding to one of the values for ΣP (Table III). The resulting prey population is then distributed randomly throughout the model domain.

A typical resultant spectrum for an overall cell concentration of 950 cells mL^{-1} is highlighted, which shows excellent agreement with the mean observed spectrum (Table III). This example spectrum has been extrapolated to the other overall cell concentration cases by applying the appropriate ratio of ΣP, in order to illustrate the range of size-partitioned forage conditions generated by the model (Table III). By assuming cells to be spheres and applying the carbon content relation of Verity *et al.* (Verity *et al.*, 1992), the full model particle spectrum (the example in Table II is an abridged form) is used to create a size-partitioned carbon content distribution (Fig. 2). The majority of the carbon potentially available for copepod ingestion in the model is within cells with *ESD* of 30 μm or smaller. However, it should be remembered that the size-based perception factor [π_1, equation (8)] prevents the mature copepods considered here from grazing on the smallest cells. It should also be noted that the procedure used to create the model particle distribution is capable of generating cells ranging up to 80-μm *ESD* in size, though the probability of these larger sizes occurring is statistically quite low.

Calibration of AOP parameter settings against observed grazing rates

Initial guesses for the AOP parameter settings were based on the characterizations of foraging behavior (Table I). Size-partitioned feeding rate measurements

Table III: Sample initial prey-size spectrum applied in the Lagrangian model

Total number of prey (ΣP)	Concentrations within size partitions (cells mL^{-1})						
	All	2–4 μm	4–6 μm	6–8 μm	8–10 μm	10–20 μm	20–40 μm
Modeled prey spectrum							
94 880	95	77.3	11.1	3.3	1.4	1.6	0.2
168 720	170	137.5	19.8	5.8	2.4	2.8	0.4
300 000	300	244.4	35.2	10.4	4.3	4.9	0.6
533 600	530	434.7	62.6	18.5	7.7	8.7	1.1
948 800	**950**	**773.0**	**111.2**	**32.9**	**13.7**	**15.5**	**2.0**
1 687 200	1700	1374.5	197.8	58.5	24.3	27.6	3.5
3 000 000	3000	2444.0	351.7	104.0	43.2	49.0	6.3
Observed prey spectrum							
Mean	905.2	690.6	145.6	37.4	14.5	16.6	0.4
SD	305.9	260.9	57.3	15.1	5.5	7.7	Not applicable

The first column in the upper portion of the table indicates the range in ΣP, that were used to initially populate the 1 Liter model domain for the experiments reported herein. This range in prey densities encompasses typical spatio-temporal variability in the open ocean. Each row illustrates a model-initialized prey spectrum for the corresponding ΣP, with the row in bold text representing a typical oligotrophic spectrum. The lower portion of the table contains the mean plankton size distribution and associated standard deviation (SD) determined from a set of recent *in situ* observations (Paffenhöfer *et al.*, 2003).

Table IV: Observed carbon uptake rates (ng C h^{-1})

Prey concentrations (cells mL^{-1})	877	834	817
Clausocalanus furcatus			
6–8 μm	2.1	1.2	2.4
8–10 μm	3.3	4.8	1.5
10–20 μm	8.3	12.8	24.1
20–40 μm	10	10	10
Paracalanus aculeatus			
6–8 μm	2.2	1.2	2.5
8–10 μm	4.2	6	1.9
10–20 μm	14.8	22.9	43.1
20–40 μm	13.4	13.4	13.4

All of the observed rates were from experiments carried out at typical oligotrophic prey concentrations, which are noted along the top row. The observed rates for *C. furcatus* were obtained during shipboard experiments carried out in the western Atlantic Ocean during June of 2001 and 2002. The rates reported for *P. aculeatus* were obtained in laboratory experiments for which the observed prey concentrations and size distributions were closely emulated (see Table IV in Paffenhöfer *et al.*, 2003).

for *C. furcatus* and *P. aculeatus* (Table IV) were used to fine-tune these parameters, where *AOI* for *C. furcatus* and *ROI* for *P. aculeatus*, respectively, were targeted (Table II). The procedure for these two species was to define a range of volume sampling rates and determine the corresponding value for their targeted AOP parameter. The range of volume sampling rates for this sensitivity analysis was 68–78 mL day^{-1} (*AOI* = 4.39–4.70°) for *C. furcatus* and 206–302 mL day^{-1} (*ROI* = 1.04–1.24 mm) for *P. aculeatus*. All of these tests were run with a 1-L control volume containing 10 copepods and an initial cell concentration of 950 cells mL^{-1}, with a total of 40 individual copepod grazing realizations acquired for each volume sampling rate tested. To assess the results of these experiments, the mean of the observed : modeled ratio of the size-partitioned carbon uptake rates (the individual rates are listed in Tables IV and V) was calculated, and the AOP setting that resulted in an overall ratio closest to 1.0, when averaged over its 40 experiments, was chosen. As reported in Table II, the best-fit volume sampling rates determined with this method were 74 mL day^{-1} for *C. furcatus* and 250 mL day^{-1} for *P. aculeatus*.

Table V: Modeled carbon uptake rates (ng C h^{-1})

Prey concentrations (cells mL^{-1})	**950**	1690	3000
Clausocalanus furcatus			
6–8 μm	**1.7**	2.9	4.8
8–10 μm	**3.5**	5.6	9.4
10–20 μm	**11.5**	18.1	28.5
20–40 μm	**12.4**	19.6	31.1
Paracalanus aculeatus			
6–8 μm	**2.8**	4.3	7.7
8–10 μm	**5.1**	8.1	14.3
10–20 μm	**16.1**	27.1	42.3
20–40 μm	**18.8**	25.7	50.2
Oithona plumifera			
6–8 μm	**0.6**	1.0	1.9
8–10 μm	**1.3**	2.2	3.8
10–20 μm	**4.7**	8.3	13.2
20–40 μm	**9.1**	16.2	21.9

The mean rates for all numerical experiments performed at the three highest prey concentrations applied in the model are shown. Values in bold indicate the concentration that is representative of typical oligotrophic conditions.

Since size-partitioned feeding rate measurements are not presently available and the hydrosensory component of its behavior is poorly understood, an alternative approach was adopted to arrive at *O. plumifera*'s best choice of parameter settings. Its sensing regions and foraging behavior were considered well characterized by the observations (Table I), so the AOP settings chosen to emulate these aspects in the model were held constant (Table II). Instead, the calibration effort targeted constraining the minimum cell velocity needed for a given particle to be 'noticed' by a given copepod. As noted earlier, this procedure made use of observations of percent body weight metabolized per day published by Klekowski *et al.* (Klekowski *et al.*, 1977). For *C. furcatus*, *P. aculeatus* and *O. plumifera*, these are 29, 17.4 and 11.5%, respectively. After applying the observed body weights (Table I), the estimated metabolic costs (in μg C day^{-1}) for the three species were 0.88, 0.81 and 0.33. Thus, the metabolic expenditure for *O. plumifera* was estimated as ~39% that of the other two species, and the minimum velocity parameter in the model was set accordingly.

Specifics of the numerical experiments

In all of the 1-h numerical experiments detailed here, 10 copepods were introduced into a model control volume of 1 L. The domain boundaries were made periodic in the sense that any particle (either prey or copepod) whose trajectory caused it to exit one side of this control volume was wrapped around so that it entered the opposite side. This feature was necessary in the case of the vertical dimension since, in initial model trials, the sinking velocity applied to all food particles resulted in either a significant loss of potential prey or a notable accumulation at the base of the model domain depending on whether passage across the bottom boundary was permitted. The initial total plankton concentration for these experiments ranged from 95 to 3000 cells mL^{-1} in order to characterize how the model-realized copepod ingestion rates change over the full range of food availability conditions (i.e. eutrophic to mesotrophic) characteristic of observed *in situ* spatiotemporal variability. Thus, in addition to the translational ambits and grazing activity of the copepod, the model tracked O (10^5–10^6) food particles in each experiment (Table III).

RESULTS

Foraging behavior

In order to fully characterize their respective sampling pathways, one experiment for each species was performed for which location and heading information for both the copepod as well as the spatial distribution of food particles was saved for every time step. The motions employed to sample the fluid medium by each copepod species are illustrated in Fig. 3, where the initial (t_0) and final (t_f) locations are indicated, and the stars indicate the copepod's location at every 100 time steps ($\Delta t = 0.5$ s). Jumps in copepod location that coincide with wrapping around the domain whenever an individual reaches a model boundary have been removed so that the ambits shown here are continuous. The inserts indicate the methods employed by each species to acquire potential food particles.

For *C. furcatus*, the sampling method consists primarily of continuous swimming at high velocity. The sampling pathway over a 5-min period from the model shows the extensive spatial range of one individual (Fig. 3a). The prominent looping aspect featured in this individual's trajectory is consistent with the ambit that has been observed for this species [see Fig. 1 in Mazzocchi and Paffenhöfer (Mazzocchi and Paffenhöfer, 1999)]. It is also worth noting that the z-axis in Fig. 3a has been compressed relative to the other two axes, so the vertical displacements that occur before reestablishing the looping motion are somewhat deemphasized. In nature, prey perception by this species is achieved by encountering cells during the extensive ambits exemplified by this trajectory realized by the model. As noted earlier, model emulated perception is necessarily different with the simulated copepod sampling a narrow, forward-extending cone at each time step.

For *P. aculeatus*, the sampling method consists of swimming continuously at low velocity while generating a feeding current that draws potential food particles toward a given individual (Fig. 3b inset). Noting that the 30-min trace of this copepod's motion can be represented in a volume that is ~3.5 times smaller than the 5-min trace shown for *C. furcatus* provides an interesting contrast between the two copepods' sampling behavior (Fig. 3a and b). Further, the path followed by *P. aculeatus* in the model does not exhibit any pronounced characteristic traits, at times pursuing a relatively straight course with slight, intermittent jogs while at other times undergoing loops of various durations (Fig. 3b).

For *O. plumifera*, the sampling method consists of settling slowly downward and employing its extensive fore and aft setae to detect prey-generated hydrodynamic signals. Interspersed between sampling periods are oblique jumps into a fresh water parcel. During these jumps, no prey is acquired. One notable characteristic of the 12-min model ambit shown in Fig. 3c is that the distance traversed by *O. plumifera* during its jumps is significantly greater than the distance covered during the settling/sampling phases of its motion. Moreover, for the most part, the individual shown here appears

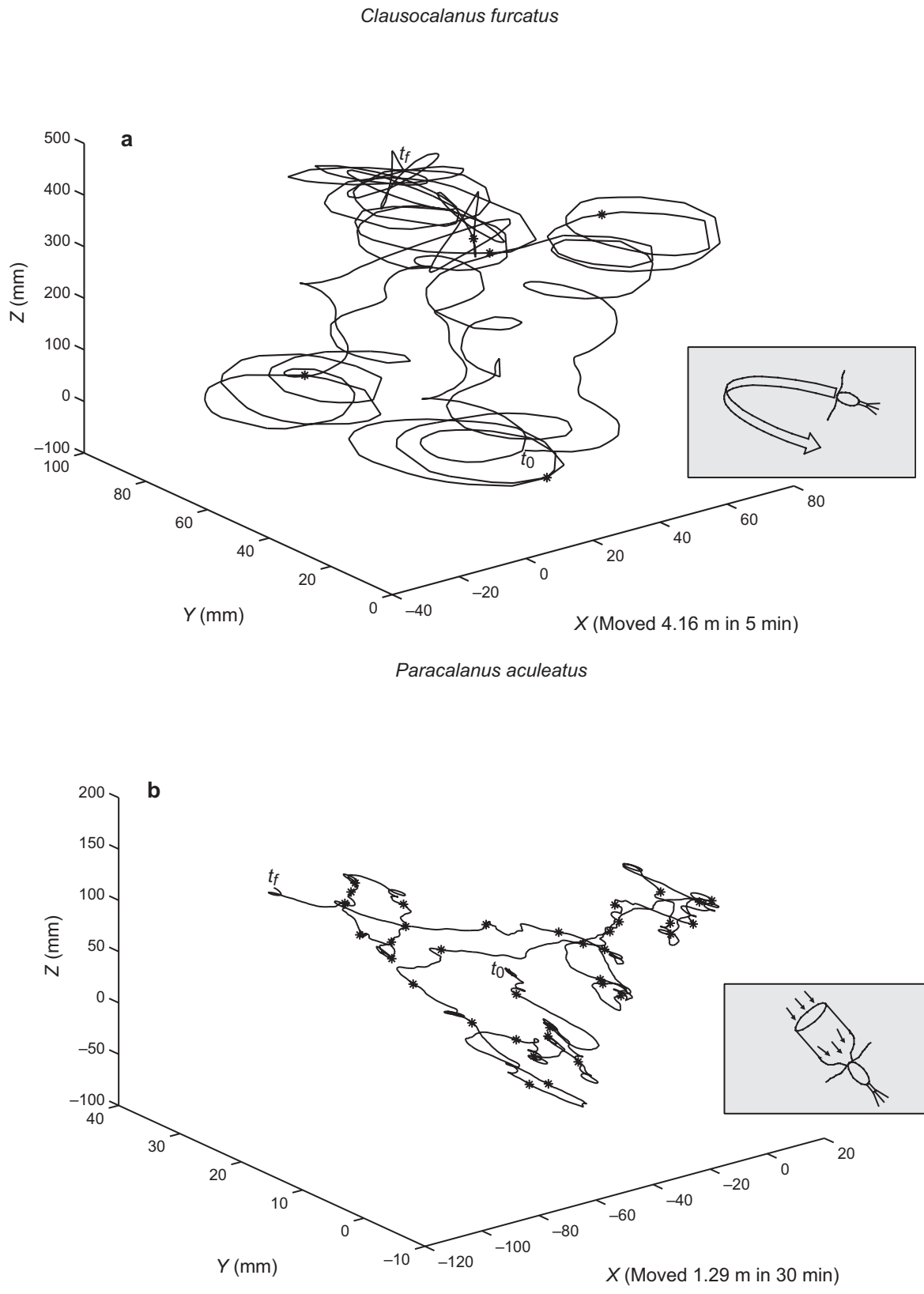

Fig. 3. Representative simulated sampling ambits for each copepod species: (**a**) *Clausocalanus furcatus*, (**b**) *Paracalanus aculeatus* and (**c**) *Oithona plumifera*. The inset illustrates the sampling method employed by each species. The amount of time represented by each track is shown, along with the distance traveled. The start (t_0) and end (t_f) points of each ambit is shown. The intermediate steps indicated by the asterisks represent the copepod's location after every 100 time steps, which here is equivalent to 50 s.

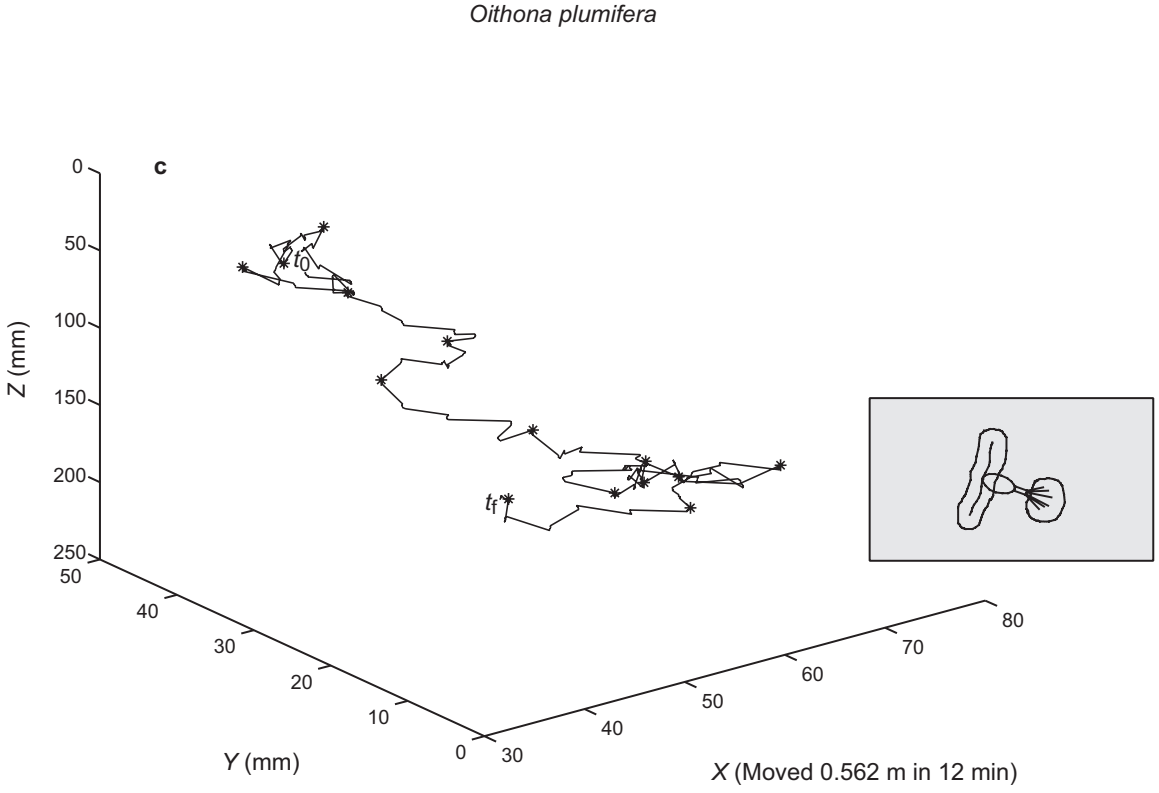

Fig. 3. continued

to succeed in moving to a completely new water parcel as a result of its jumps, although some overlap may occur near its initial position and toward the end of the ambit shown (Fig. 3c).

Grazing characteristics over the full range of prey concentrations

In Fig. 4, curves illustrating size-partitioned ingestion rate in ng C h^{-1} for the three highest prey concentrations are shown for each species. The modeled rates shown here are the mean values for all experiments performed at each prey concentration. At the smaller particle sizes, each curve increases monotonically with prey *ESD*. Both *C. furcatus* and *P. aculeatus* reach an asymptote at the 10- to 20-μm partition, while *O. plumifera*'s rate continues to rise. These curves also indicate that the degree that size-specific ingestion rates increase as the prey population increases is relatively consistent across all size partitions. To quantify this trend, these model results are listed in Table V. Further, it should be noted that for the three highest prey concentrations, the percent increase in concentration between each case is identical (i.e. 78%; Table III). As total prey concentration increases from 950 to 1700 cells mL^{-1}, the mean increase in ingestion rate across all size partitions ranges from 55 to 72% for the three species, whereas when prey concentration is increased from 1700 to 3000 cells mL^{-1}, mean ingestion rate increases from 63 to 76%.

Observed ingestion rates for *C. furcatus* and *P. aculeatus* are shown (open circles, Fig. 4a and b). These rates are listed in Table V. The measured rates for these two species are fairly close in magnitude, with *P. aculeatus* exhibiting a mean rate over all size classes that is ~35% higher for cell concentrations ranging from 817 to 877 cells mL^{-1} (Table IV). The size-partitioned measurements also indicate that the two species exhibit little difference in carbon contributed by the smallest cells, while *P. aculeatus* shows a 79% greater contribution to its carbon diet by cells within the 10- to 20-μm partition. In the model, the overall ingestion rate for *P. aculeatus* is ~50% higher than for *C. furcatus*. Moreover, *P. aculeatus* obtains 60% more carbon from the 6- to 8-μm partition, whereas the contribution to its carbon diet by cells within the 10- to 20-μm partition is only 40% greater than that for *C. furcatus*. So based on the observations in Tables IV and V, the

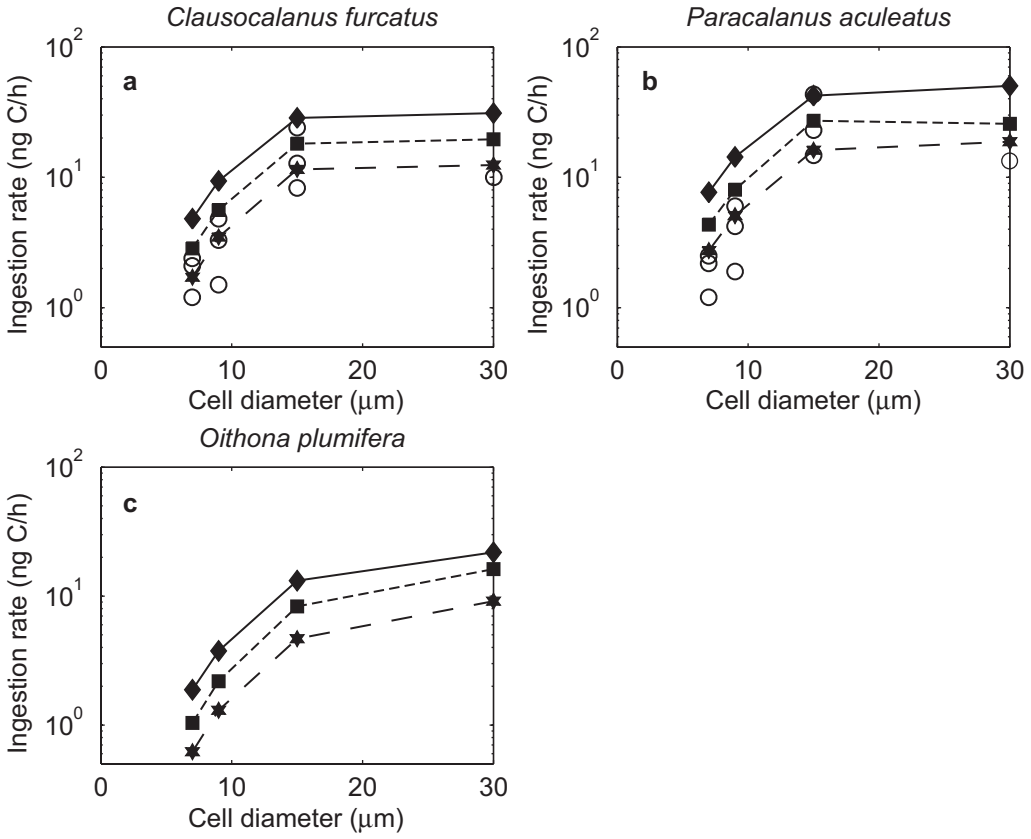

Fig. 4. Size-differentiated ingestion rate (ng C h^{-1}) at three initial prey concentrations (*P*): (**a**) *Clausocalanus furcatus*, (**b**) *Paracalanus aculeatus* and (**c**) *Oithona plumifera*. The three initial *P* are 950 cells/mL (— ✸ —), 1690 cells/mL (– – ■ – –) and 3000 cells/mL (—◆—). The lowest concentration is consistent with the observed *P* reported in Table III. The observed ingestion rates shown in **a** and **b** (○) are from Table IV.

model appears to overemphasize the relative contribution of carbon made by small cells and underemphasize the contribution of 10- to 20-μm cells to the diet of *P. aculeatus* in comparison with *C. furcatus*.

As described in *Calibration of AOP parameter settings against observed grazing rates*, the magnitude of modeled uptake by *O. plumifera* has been constrained as well as is currently possible. Nevertheless, the relative ingestion rates apparent in the model results provide some interesting contrasts between the grazing characteristics of the three species. For instance, while *O. plumifera* exhibits lower ingestion rates for all size classes and prey concentrations, the difference in rates always becomes less pronounced as prey *ESD* increases, and the smallest rate differences always coincide with the largest cells (Table V). Another interesting model characteristic is that at the higher prey concentrations, the difference in carbon uptake rate between *O. plumifera* and the other two species is ~15% lower than at 950 cells mL^{-1}.

For all three species, the model exhibits a direct relation between overall carbon uptake rate (i.e. not size partitioned) and prey concentration (Fig. 5). Not surprisingly, a slope of nearly one is obtained for all three species when a linear fit (not shown) is applied to the log transform of the modeled mean ingestion rates (the mean rates at each prey concentration are connected by the solid lines in Fig. 5). SDs of the data in Fig. 5 demonstrate that the modeled rates for *P. aculeatus* always exhibit the greatest scatter while *C. furcatus* and *O. plumifera* are evenly split as to which exhibits the least. The direct relation between uptake rate and prey concentration, as well as the magnitude of modeled carbon uptake, is consistent with recently measured rates obtained from grazing experiments carried out with *C. furcatus* and *P. aculeatus* (Paffenhöfer, Mazzocchi and Tzeng, unpublished data). In addition to matching the observed trend and magnitude, for a concentration of 950 cells mL^{-1}, the range of modeled ingestion rate for *C. furcatus* and *P. aculeatus* is consistent with these measurements.

Grazing characteristics at typical oligotrophic prey concentrations

In all of the results to follow, the standard oligotrophic condition for cell concentration (950 cells/mL)

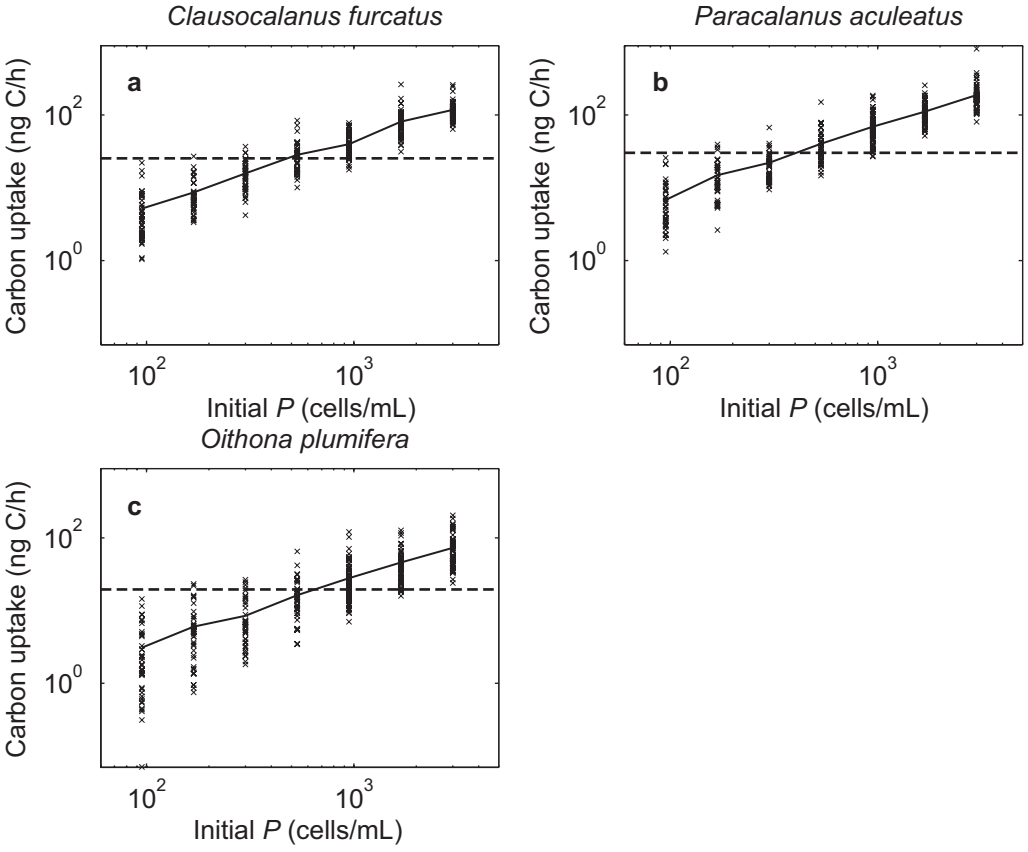

Fig. 5. Ingestion rate (ng C h^{-1}) with varying initial prey concentration (P) for each copepod species: (**a**) *Clausocalanus furcatus*, (**b**) *Paracalanus aculeatus* and (**c**) *Oithona plumifera*. The solid line shows how the mean ingestion rate for each case varies with concentration. Except for the realistic case of 950 cells mL^{-1} for which additional realizations were obtained (Fig. 6), 10 experiments were performed at each concentration. All individual results are shown (×). The dashed line represents the estimate of each copepod's metabolic rate that is based on the observed weight for each species and the environmental temperature (Ikeda, 1985).

has been applied. The mean rate of cell consumption ealized by the model is 154 cells h^{-1} for *C. furcatus*, 229 cells h^{-1} for *P. aculeatus* and 62 cells h^{-1} for *O. plumifera* (Fig. 6). The histograms in Fig. 6 illustrate the difference in these mean rates as they show each species occupying a largely distinct range of cell consumption rate with little overlap. The cell consumption rate for *P. aculeatus* exhibits the widest range (Fig. 6b), with minimum and maximum values of 172 and 286 cells h^{-1}. These rates are somewhat higher than those observed when a diet consisting solely of the diatom *Thalassiosira eccentrica* (*ESD* = 34–41 μm) was offered to *P. aculeatus* in laboratory experiments (Paffenhöfer *et al.*, 1995). The shape of this species' modeled rate distribution is also the least Gaussian. The main peak represents 17% of the occurrences while a secondary peak, which is five bins removed, accounts for 11% of the occurrences. The distributions for *C. furcatus* and *O. plumifera* exhibit a more typical Gaussian character with their main peaks representing 24 and 40% of the occurrences, respectively (Fig. 6a and c). The range in consumption rate for *C. furcatus* (122–193 cells h^{-1}) is somewhat larger than that of *O. plumifera* (42–87 cells h^{-1}).

In Fig. 7, for each size class, the percent contribution to total cells consumed by *C. furcatus* is shown. The width of each partition in this histogram is 4 μm. The 8- to 12-μm partition makes the largest contribution to total uptake, accounting for 49% of the cells grazed. The secondary peak coincides with the 4- to 8-μm partition, which contributes 26% of the total number of grazed cells. While prey in this partition are plentiful (Table III), the size-based perception factor imposed on copepod grazing by π_1 [equation (8)] prevents these small cells from making a more significant contribution. The magnitude of the contribution of the larger size partitions decreases monotonically in a manner consistent with the size distribution of the prey population (Table III). To highlight species-specific differences, the distribution in Fig. 7 has been subtracted from the corresponding

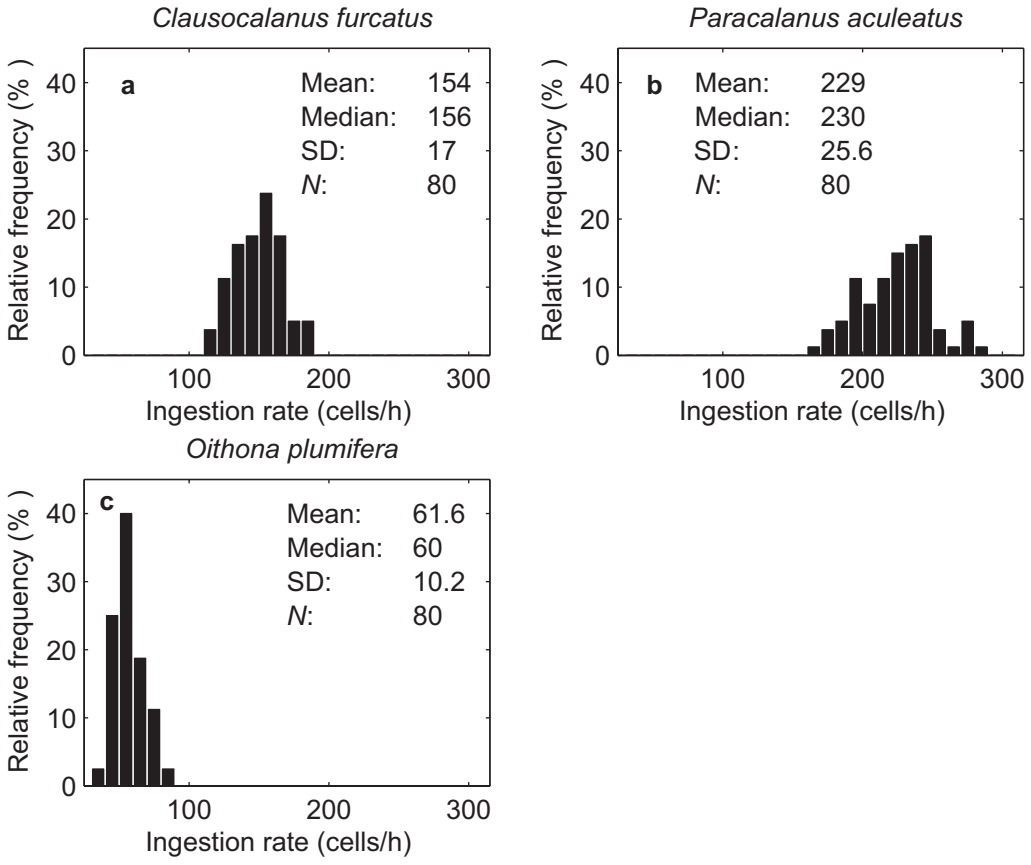

Fig. 6. Histograms of ingestion rate (cells h^{-1}) realized for all experiments performed for each copepod species: (**a**) *Clausocalanus furcatus*, (**b**) *Paracalanus aculeatus* and (**c**) *Oithona plumifera*. The mean, median, SD and number of experiments are provided. All experiments were performed with an initial prey concentration (P) of 950 cells mL^{-1}. The bin size for these histograms is 10 cells h^{-1}.

distributions for the other two species. In Fig. 8a, the difference distribution indicates that smaller cells constitute a greater portion of the diet of *P. aculeatus*, and this is compensated for by a relatively smaller contribution by cells with *ESD* of 8–12 μm. The model also indicates that cells with *ESD* >12 μm made essentially comparable contributions to the diet of these two species (Fig. 8a). In Fig. 8b, the difference distribution indicates that cells with *ESD* >12 μm made a greater relative contribution to the diet of *O. plumifera*. This compensates for the less prominent contribution made by cells in the 4- to 8- and 8- to 12-μm partitions.

In Fig. 9, total carbon uptake as a function of size partition is shown for the three species, and the contribution by cells with *ESD* ranging up to 80 μm has been included. These histograms show that the 8- to 12-μm partition always makes the largest contribution to the overall carbon budget of each species, though this generalization barely holds for *O. plumifera* (Fig. 9). In addition, total carbon uptake by *P. aculeatus* is nearly always highest for all size classes while for *O. plumifera* it is always lowest. It can also be seen that for *O. plumifera*, the contribution by the various size classes is relatively uniform, whereas for the other two species there is a pronounced decrease in the contribution made by the 8- to 12-μm partition and the larger cells. This indicates that the small cells make a proportionally greater contribution to the carbon uptake budgets of *C. furcatus* and, especially, *P. aculeatus*.

To investigate the dietary implication of this size preference, the percent contribution to carbon uptake as a function of size class has been determined for each copepod species (Fig. 10). Here the size partitions have been made consistent with those utilized when comparing with the observational data shown in Fig. 4, with the addition of a 10- to 12-μm partition to contrast with the 8- to 10-μm partition and a 40- to 80-μm partition to characterize the contribution of the largest cells. For the evenly spaced partitions for plankton with *ESD* up to 12 μm, the 8- to 10-μm partition consistently makes the highest contribution to each species' carbon uptake (Fig. 10). Thus when cells are sorted within

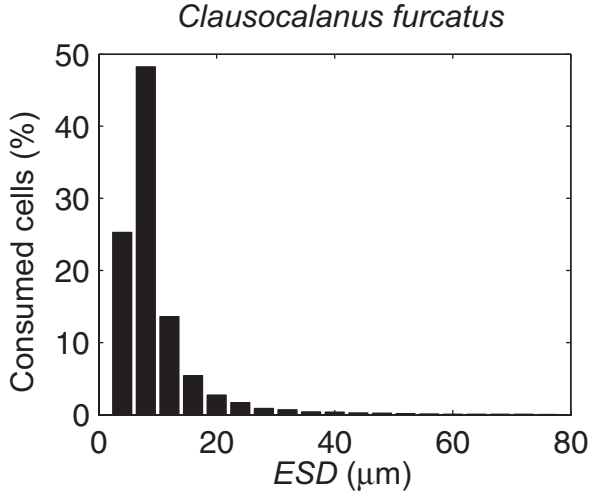

Fig. 7. Histogram, for *Clausocalanus furcatus*, of the percent contribution of a given size partition to the total number of cells consumed. The size of each partition is 4 μm. This is the averaged distribution ($n = 80$) for all experiments where the initial prey concentration (P) was 950 cells mL^{-1}.

evenly divided 2-μm bins, plankton within the 8- to 10-μm partition are the dominant source of carbon for all three copepod species. For the three broader size partitions, the percentage of carbon uptake contributed to the diet of each species increases monotonically along with the bounds of each partition. For the three species, the contribution by the 10- to 20-, 20- to 40- and 40- to 80-μm partitions ranges from 18 to 26, 28 to 33 and 32 to 41%, respectively (Fig. 10). However, when these are normalized to coincide with a 2-μm bin width, the percent contribution is <3% in all cases and is therefore lower than the contribution provided by prey within the 8- to 10-μm partition. These distributions also demonstrate that *O. plumifera* has a greater dependence on cells within the two largest size partitions to fulfill its nutritional needs, while the other two species depend more heavily on prey with *ESD* <20 μm (Fig. 10). The relative contribution of these partitions to the diet of each species illustrated by Fig. 10 is consistent with the size-differentiated distributions of cell consumption rate and carbon uptake described above (Figs 8 and 9).

Metabolic requirements

The distributions in Fig. 10 show how the various-sized plankton contribute to the carbon uptake budget of each modeled copepod species. However, they do not indicate whether this uptake is sufficient to satisfy basal metabolic needs or the additional requirements imposed by reproduction. Estimates of metabolic cost have been obtained for each copepod species by applying an empirical relation that depends on stipulating an *in situ* temperature (here taken as 20°C) and providing a characteristic weight (Ikeda, 1985). The copepod weights used in this estimate are listed in Table I. The dashed lines on each panel of Fig. 5 indicate the resulting estimate of metabolic cost for each species.

For all three species, the mean rate of carbon uptake does not meet or exceed the weight-based minimum metabolic cost below prey concentrations of 530 cells mL^{-1} (Fig. 5). Further, *O. plumifera*'s mean uptake is just below its estimated cost at this concentration, whereas the two other species are just above their basal needs.

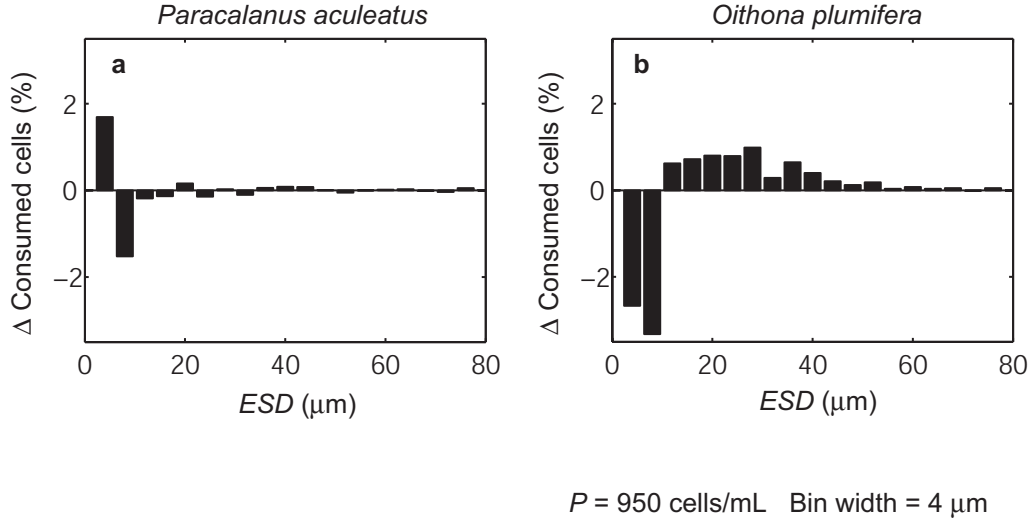

Fig. 8. Difference histograms of the percent contribution to total consumed cells by size class for (**a**) *Paracalanus aculeatus* and (**b**) *Oithona plumifera*, where the histogram for *Clausocalanus furcatus* shown in Fig. 7 has been subtracted from the corresponding distribution for the other two species. Otherwise, the details of these two histograms are as described in the caption for Fig. 7.

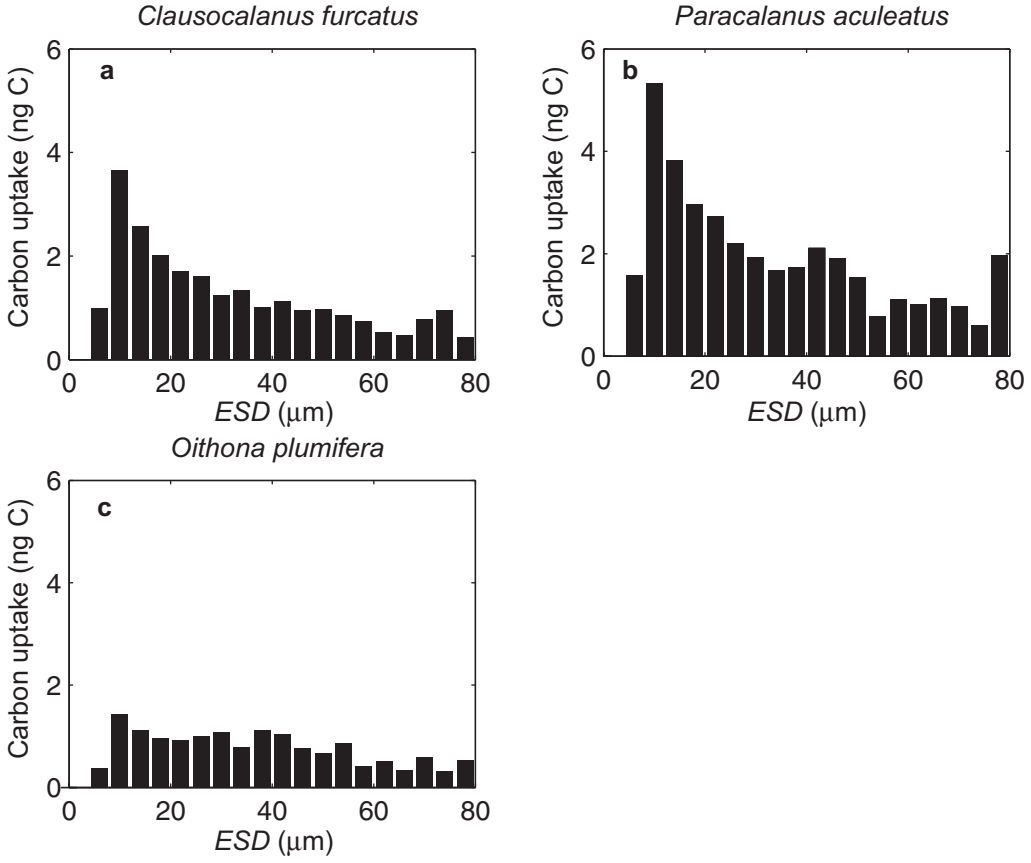

Fig. 9. Histogram of percentage of total carbon contributed to total uptake as a function of cell size for (**a**) *Clausocalanus furcatus*, (**b**) *Paracalanus aculeatus* and (**c**) *Oithona plumifera*. These are the averaged size-differentiated contributions for all experiments where the initial prey concentration (*P*) was 950 cells mL^{-1}. The total carbon uptake for this *P* is shown graphically in Fig. 5. The upper equivalent cell diameter (*ESD*) limit has been extended to illustrate that, despite their relatively low population density, these larger cells make a significant contribution to total carbon acquired by all three copepod species. The bin size for these histograms is 4 μm.

None of the three species manage to achieve or exceed their estimated metabolic cost at the lowest prey concentration. For *C. furcatus*, there is only one instance at 170 cells mL^{-1}, and two instances at 300 cells mL^{-1}, for which the modeled uptake rate exceeded its cost threshold (Fig. 5a). For *P. aculeatus*, there are several instances where this threshold is achieved at both of these low concentrations (Fig. 5b). For *O. plumifera*, 10% of the carbon uptake rates at 170 cells mL^{-1} are <1 ng C h^{-1} while at the lowest concentration fully 30% of the realized uptake rates are below this threshold (Fig. 5c).

DISCUSSION

Initial results from a stochastic, three-dimensional Lagrangian particle model have been presented. While there have been past efforts that adopted a similar approach (Caparroy, 2004), to our knowledge the model described here is the first to include a variety of explicit copepod foraging behaviors. The three species of copepod whose feeding and behavioral dynamics have been simulated in this individual-based model (IBM) are *C. furcatus*, *P. aculeatus* and *O. plumifera*. For the two former species, detailed measurements of grazing rates obtained during recent shipboard and laboratory experiments have been utilized to tune their AOP settings (Table IV). However, it was found that this tuning only marginally improved the model's skill when compared with simulations that used the initial guesses for AOP settings based on careful behavioral characterizations. This is indicative of the future potential for this type of IBM as an environmental modeling tool. Similar grazing rate measurements for *O. plumifera* are not presently available, so its parameter tuning was made in relation to the other two species that were better constrained. Furthermore, the least understood aspect of its foraging behavior relates to sensitivity to hydrodynamic stimuli. Therefore, AOP settings based solely on

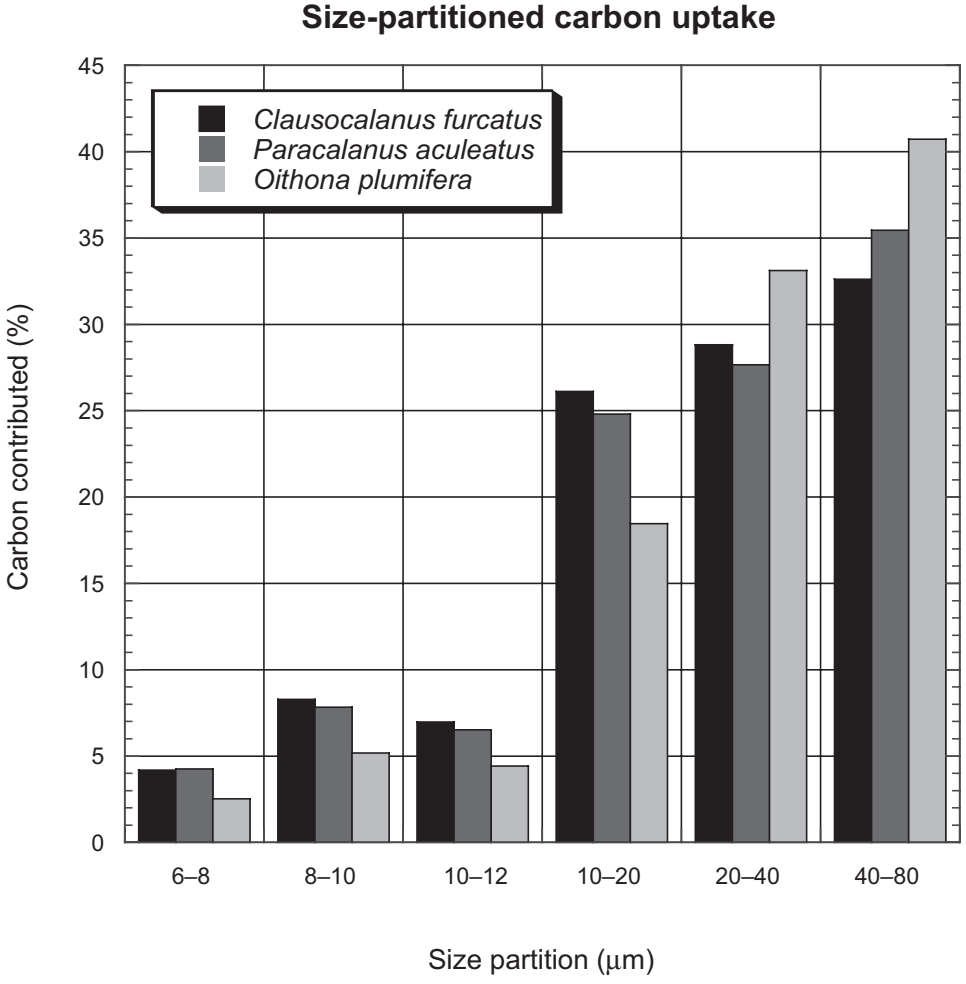

Fig. 10. Percentage of total carbon uptake that is provided to each copepod species by plankton within six size partitions. The partition definitions are consistent with those applied to the observations included on Fig. 4 with the addition of the 10- to 12-μm partition to provide a comparison to the 8- to 10-μm partition and the 40- to 80-μm partition that characterizes the contribution of the largest cells.

observational characterizations were applied (an assumption supported by the just noted experience with the other two species), and a minimum particle velocity threshold was ascertained by applying published observations of percent body weight metabolized per day for all three species (Klekowski *et al.*, 1977).

Since the method for defining each species' sensing regions has been kept relatively simple (Fig. 1), precisely emulating observed AOP configurations was not feasible. However, volume sampling by each species is always consistent with the observed rate (Tables I and II). Another aspect of the model that was crucial for realistically emulating the pelagic environment was initializing the prey field's size distribution. Here again, the availability of good quality *in situ* measurements was invaluable (Paffenhöfer *et al.*, 2003), as the empirical relation determined from these data was applied to transform the model-generated set of uniform deviates into a realistic plankton size spectrum. There are several additional stochastic aspects to the model. These include initializing the spatial distribution of all particles, diffusing the prey through the model domain as time evolves and continually modifying the timing and magnitude of directional changes applied to each copepod's ambit. While the randomness introduced by these model functionalities necessitated performing numerous simulations in order to obtain well-characterized results, this feature of the model was crucial for emulating intrinsic oceanic biological variability.

The distinct sampling behavior of each species results in notably different uptake characteristics. The fast, continuous ambit of *C. furcatus* leads to a preference for medium-sized prey (8–40 μm) while the feeding current

and slow continuous motion of *P. aculeatus* results in a preference for the smallest cells. Furthermore, the model results indicate that the relatively stationary sampling techniques employed by *P. aculeatus* and, especially, *O. plumifera* are better suited for encountering the largest cells that feature elevated sinking velocities. In the case of *O. plumifera*, the preference for large cells is accentuated by the strong hydrodynamic signal that their sinking produces. The highest rate of cell consumption is exhibited by *P. aculeatus*, though much of this additional uptake is comprised of small cells that do not appreciably add to its carbon budget. This species also exhibits the greatest SD in uptake rates at all prey concentrations, which suggests its sensitivity to prey patchiness is more pronounced.

The model results suggest that *P. aculeatus* is the species most likely to persist as oligotrophy becomes acute, whereas *O. plumifera* appears to be less likely to be able to acquire its metabolic needs as prey concentrations are reduced (Fig. 5). However, a prey concentration of 530 cells mL^{-1} represents a forage availability threshold above which all three species generally meet their basal metabolic needs. Additional experiments demonstrate that including only one adult copepod per liter results in cell ingestion rate distributions (not shown) that are statistically identical to those obtained when there are 10 copepods per liter (Fig. 6). Thus it appears that adult copepod populations in the oligotrophic environment are limited by prey concentration and/or predation but not by resource competition. However, the question of whether resource competition plays an active role in prescribing the magnitude of copepod populations must remain open since the model does not yet include the full range of copepodite stages [e.g. as described within a modeling context by Soussi and Bernard (Soussi and Bernard, 2004)]. The present model configuration also has no restriction on the maximum prey size that can be ingested by the virtual copepods; rather, the infrequent occurrence of plankton >70 μm in the generated prey spectra has been the primary means of limiting the uptake of these cells. One study has suggested the existence of a quasi-universal scaling based on prey *ESD* normalized by copepod prosome length that could provide an upper cell size limit (Berggreen *et al.*, 1988). Employing such a threshold could be included relatively easily by making d_P [equation (8)] a function of copepod size.

At the lowest prey concentrations, *O. plumifera* is the only species that exhibits difficulty in maintaining carbon uptake >1 ng C h^{-1}. This is an order of magnitude less than its estimated metabolic cost and suggests that this species is the most likely to employ energy conserving behavior. This is a direct result of its model-indicated preference for large cells, which relates to cell velocities being primarily linked to *ESD*-prescribed sinking [equation (2)]. Without a more comprehensive characterization of *O. plumifera*'s sensory capabilities, this species' preference for fast-sinking or motile cells is uncorroborated. However, it should be noted that *Oithona* spp. has been shown to prefer motile prey over diatoms during the spring in polar regions [(Atkinson, 1998) and references within]. Thus, applying a plankton spectrum that includes both passive and motile prey would allow for more realistically emulating prey detection and grazing rates by copepods that rely on perceiving hydrodynamic signals. Incorporating such an enhancement, along with providing for a full complement of copepodites with preferred prey size coupled to prosome length (i.e. growth stage), would result in a modeling tool that could be used to investigate how predation and resource limitation/competition impact copepod population densities in both oligotrophic and neritic environments.

This modeling effort makes use of the best available information and though it has limitations, it is also a first attempt at simulating explicit foraging behavior for several common copepod species. Our study depends crucially on detailed observations of the sampling behavior and grazing characteristics of these species. Ultimately, extending the utility and realism of this model will require further careful behavioral analyses. Characterization of copepod perception over distance and how this is affected by prey concentration or turbulence would be especially beneficial, though as noted by Haury and Yamazaki (Haury and Yamazaki, 1995) basing copepod perception distance on demonstrative behavioral response is potentially misleading. Turbulence in the marine environment affects copepods and their foraging mechanisms in a variety of ways. These impacts include increased metabolism as swimming patterns are modified, and heartbeat rates become elevated (Alcaraz, 1997); modification of predator–prey encounter rates (Rothschild and Osborn, 1988; Marrasé *et al.*, 1990; Seuront *et al.*, 2001); and disruption of feeding currents, though Yen (Yen, 2000) has argued that the intermittent nature of turbulence allows copepod-generated laminar flows to be quickly reestablished. The model presented here is well suited for exploring how various levels of turbulent dissipation rate will affect predator–prey encounter rates, either through modifying the value of D in equation (3) or by directly coupling this IBM to a turbulence closure model that can provide spatially and temporally varying turbulent diffusivities [e.g. similar to ecosystem coupling employed by Wiggert *et al.* (Wiggert *et al.*, 2000)].

Overall, the model demonstrates that, even though they access distinct subdomains of the prey spectrum,

the three copepod species considered have the same prey availability threshold above which they are able to satisfy their metabolic needs. This implies that the size-partition preferences resulting from their different foraging behavior contribute to their coexistence in the dilute prey environment that they inhabit (i.e. Hutchinson's paradox). Looking forward, an expected benefit of this behaviorally explicit grazing model is to facilitate the introduction of greater realism into the continuum-based ecosystems currently incorporated within three-dimensional coupled biogeochemical–physical models. The zooplankton component of these model ecosystems typically functions as a catchall means of mathematical closure, and developing ways of incorporating more realistic grazing behavior is a critical need (Flierl *et al.*, 1999; Fennel, 2001). Finally, the contribution of meta- and mesozooplankton respiration to the global oceanic carbon budget is generally disregarded, even though a recent estimate of the latter has placed it at 13 Gt C $year^{-1}$ (Hernández-León and Ikeda, 2005), which is ~25% of the current estimate for global primary production. Thus, a number of significant benefits should be realized by developing modeling techniques that more accurately account for the role of copepods in the pelagic system.

ACKNOWLEDGEMENTS

The National Oceanographic Partnership Program supported this research (grant number N00014-02-1-0370). Computer facilities and support were provided by the Commonwealth Center for Coastal Physical Oceanography at Old Dominion University. The thoughtful suggestions of two anonymous reviewers helped strengthen this report and are greatly appreciated. We would also like to thank Roger Harris for his efforts as special editor of the Paffenhöfer section.

REFERENCES

Alcaraz, M. (1997) Copepods under turbulence: grazing, behavior and metabolic rates. *Sci. Mar.*, **61**, 177–195.

Al-Mutairi, H. and Landry, M. R. (2001) Active export of carbon and nitrogen at Station ALOHA by diel migrant zooplankton. *Deep-Sea Res. II*, **48**, 2083–2103.

Atkinson, A. (1998) Life cycle strategies of epipelagic copepods in the southern ocean. *J. Mar. Syst.*, **15**, 289–311.

Banse, K. (1994) On the coupling of hydrography, phytoplankton, zooplankton, and settling organic particles offshore in the Arabian Sea. *Proc. Indian Acad. Sci., Earth Planet. Sci.*, **103**, 125–161.

Bartram, W. C. (1980) Experimental development of a model for the feeding of neritic copepods on phytoplankton. *J. Plankton Res.*, **3**, 25–51.

Berggreen, U., Hansen, B. and Kiørboe, T. (1988) Food size spectra, ingestion and growth of the copepod *Acartia tonsa* during development: implications for determination of copepod production. *Mar. Biol.*, **99**, 341–352.

Calbet, A. and Landry, M. R. (1999) Mesozooplankton influences on the microbial food web: direct and indirect trophic interactions in the oligotrophic open ocean. *Limnol. Oceanogr.*, **44**, 1370–1380.

Caparroy, P. (2004) Discrete events-based Lagrangian approach as a tool for modeling predator-prey interactions in the plankton. In Seuront, L. and Strutton, P. G. (eds), *Handbook of Scaling Methods in Aquatic Ecology: Measurement, Analysis, Simulation*. CRC Press, Boca Raton, FL, pp. 559–573.

Cowles, T. J. and Fessenden, L. M. (1995) Copepod grazing and fine-scale distribution patterns during the Marine Light-Mixed Layers experiment. *J. Geophys. Res.*, **100**, 6677–6686.

Fennel, W. (2001) Modeling of copepods with links to circulation models. *J. Plankton Res.*, **23**, 1217–1232.

Flierl, G., Grünbaum, D., Levin, S. *et al.* (1999) From individuals to aggregations: the interplay between behavior and physics. *J. Theor. Biol.*, **196**, 397–454.

Gallienne, C. P. and Robins, D. B. (2001) Is *Oithona* the most important copepod in the world's oceans? *J. Plankton Res.*, **23**, 1421–1432.

Gaudy, R., Champalbert, G. and Le Borgne, R. (2003) Feeding and metabolism of mesozooplankton in the equatorial pacific high-nutrient, low-chlorophyll zone along 180 degrees. *J. Geophys. Res.*, **108**, doi:10.1029/2000 JC 000743.

Ghilarov, A. M. (1984) The paradox of the plankton reconsidered; or, why do species coexist? *Oikos*, **43**, 46–52.

Haury, L. R. and Yamazaki, H. (1995) The dichotomy of scales in the perception and aggregation behavior of zooplankton. *J. Plankton Res.*, **17**, 191–197.

Hayward, T. L. and McGowan, J. A. (1979) Pattern and structure in an oceanic zooplankton community. *Am. Zool.*, **19**, 1045–1055.

Hernández-León, S. and Ikeda, T. (2005) A global assessment of mesozooplankton respiration in the ocean. *J. Plankton Res.*, **27**, 153–158.

Huskin, I., Viesca, L. and Anadón, R. (2004) Particle flux in the subtropical Atlantic near the Azores: influence of mesozooplankton. *J. Plankton Res.*, **26**, 403–415.

Hutchinson, G. E. (1961) The paradox of the plankton. *Am. Nat.*, **XCV**, 137–145.

Ikeda, T. (1985) Metabolic rates of epipelagic marine zooplankton as a function of body mass and temperature. *Mar. Biol.*, **85**, 1–11.

Klekowski, R. Z., Kukina, I. V. and Tumanseva, N. I. (1977) Respiration in the microzooplankton of the equatorial upwellings in the eastern Pacific Ocean. *Pol. Arch. Hydrobiol.*, **24**, 467–489.

Kleppel, G. S. (1993) On the diets of calanoid copepods. *Mar. Ecol. Prog. Ser.*, **99**, 183–195.

Longhurst, A. R. (1985) Relationship between diversity and the vertical structure of the upper ocean. *Deep-Sea Res. I*, **32**, 1535–1570.

Mann, K. H. and Lazier, J. R. N. (1996) *Dynamics of Marine Ecosystems: Biological-Physical Interactions in the Ocean*. Blackwell Science, Cambridge, MA.

Marine Zooplankton Colloquium 2. (2001) Future marine zooplankton research – a perspective. *Mar. Ecol. Prog. Ser.*, **222**, 297–308.

Marrasé, C., Costello, J. H., Granata, T. *et al.* (1990) Grazing in a turbulent environment: energy dissipation, encounter rates, and

efficacy of feeding currents in *Centropages hamatus*. *Proc. Natl. Acad. Sci. U. S. A.*, **87**, 1653–1657.

Mazzocchi, M. G. and Paffenhöfer, G. A. (1998) First observations on the biology of *Clausocalanus furcatus* (Copepoda, Calanoida). *J. Plankton Res.*, **20**, 331–342.

Mazzocchi, M. G. and Paffenhöfer, G. A. (1999) Swimming and feeding behaviour of the planktonic copepod *Clausocalanus furcatus*. *J. Plankton Res.*, **21**, 1501–1518.

McGowan, J. A. and Walker, P. W. (1985) Dominance and diversity maintenance in an oceanic ecosystem. *Ecol. Monogr.*, **55**, 103–118.

McManus, M. A., Alldredge, A. L., Barnard, A. *et al.* (2003) Characteristics, distribution and persistence of thin layers over a 48 hour period. *Mar. Ecol. Prog. Ser.*, **261**, 1–19.

Nival, P. and Nival, S. (1976) Particle retention efficiencies of an herbivorous copepod, *Acartia clausi* (adult and copepodite stages): effects on grazing. *Limnol. Oceanogr.*, **21**, 24–38.

Padisák, J., Soróczki-Pintér, É. and Rezner, Z. (2003) Sinking properties of some phytoplankton shapes and the relation of form resistance to morphological diversity of plankton – an experimental study. *Hydrobiologia*, **500**, 243–257.

Paffenhöfer, G. A. (1984) Does *Paracalanus* feed with a leaky sieve? *Limnol. Oceanogr.*, **29**, 155–160.

Paffenhöfer, G. A. (1993) On the ecology of marine cyclopoid copepods (Crustacea, Copepoda). *J. Plankton Res.*, **15**, 37–55.

Paffenhöfer, G. A. (1998) On the relation of structure, perception and activity in marine planktonic copepods. *J. Mar. Syst.*, **15**, 457–473.

Paffenhöfer, G. A., Bundy, M. H., Lewis, K. D. *et al.* (1995) Rates of ingestion and their variability between individual calanoid copepods: direct observations. *J. Plankton Res.*, **17**, 1573–1585.

Paffenhöfer, G. A. and Mazzocchi, M. G. (2002) On some aspects of the behaviour of *Oithona plumifera* (Copepoda: Cyclopoida). *J. Plankton Res.*, **24**, 129–135.

Paffenhöfer, G. A., Tzeng, M., Hristov, R. *et al.* (2003) Abundance and distribution of nanoplankton in the epipelagic subtropical/tropical open Atlantic Ocean. *J. Plankton Res.*, **25**, 1535–1549.

Richerson, P., Armstrong, R. and Goldman, C. R. (1970) Contemporaneous disequilibrium, a new hypothesis to explain the "paradox of the plankton". *Proc. Natl. Acad. Sci. U. S. A.*, **67**, 1710–1714.

Roman, M. R. (1984) Utilization of detritus by the copepod, *Acartia tonsa*. *Limnol. Oceanogr.*, **29**, 949–959.

Roman, M. R., Caron, D. A., Kremer, P. *et al.* (1995) Spatial and temporal changes in the partitioning of organic carbon in the plankton community of the Sargasso Sea off Bermuda. *Deep-Sea Res. I*, **42**, 973–992.

Roman, M. R. and Gauzens, A. L. (1997) Copepod grazing in the equatorial Pacific. *Limnol. Oceanogr.*, **42**, 623–634.

Rothschild, B. J. and Osborn, T. R. (1988) Small-scale turbulence and plankton contact rates. *J. Plankton Res.*, **10**, 465–474.

Seuront, L., Schmitt, F. and Lagadeuc, Y. (2001) Turbulence intermittency, small-scale phytoplankton patchiness and encounter rates in plankton, where do we go from here? *Deep-Sea Res. I*, **48**, 1199–1215.

Soussi, S. and Bernard, O. (2004) Identification of interactions in copepod populations using a qualitative study of stage-structured population models. In Seuront, L. and Strutton, P. G. (eds), *Handbook of Scaling Methods in Aquatic Ecology: Measurement, Analysis, Simulation*. CRC Press, Boca Raton, FL, pp. 361–379.

Svensen, C. and Kiørboe, T. (2000) Remote prey detection in *Oithona similis*: hydromechanical versus chemical cues. *J. Plankton Res.*, **22**, 1155–1166.

Svensen, C. and Nejstgaard, J. C. (2003) Is sedimentation of copepod faecal pellets determined by cyclopoids? Evidence from enclosed ecosystems. *J. Plankton Res.*, **25**, 917–926.

Verity, P. G., Robertson, C. Y., Tronzo, C. R. *et al.* (1992) Relationships between cell volume and the carbon and nitrogen content of marine photosynthetic nanoplankton. *Limnol. Oceanogr.*, **37**, 1434–1446.

Wiggert, J. D., Jones, B. H., Dickey, T. D. *et al.* (2000) The northeast monsoon's impact on mixing, phytoplankton biomass and nutrient cycling in the Arabian Sea. *Deep-Sea Res. II*, **47**, 1353–1385.

Yen, J. (2000) Life in transition: balancing inertial and viscous forces by planktonic copepods. *Biol. Bull.*, **198**, 213–224.